Title

Putative receptor binding sites on alphaviruses as visualized by cryoelectron microscopy.

Journal

Proceedings of the National Academy of Sciences of the United States of America, 92(23)

ISSN

0027-8424

Authors

Smith, TJ
Cheng, RH
Olson, NH
et al.

Publication Date

1995-11-07

DOI

10.1073/pnas.92.23.10648

Peer reviewed

Proc. Natl. Acad. Sci. USA
Vol. 92, pp. 10648–10652, November 1995
Immunology

Putative receptor binding sites on alphaviruses as visualized by cryoelectron microscopy

(antibodies/neutralization/Sindbis virus/Ross River virus)

THOMAS J. SMITH*, R. HOLLAND CHENG, NORMAN H. OLSON, PETER PETERSON, ELAINE CHASE, RICHARD J. KUHN, AND TIMOTHY S. BAKER

Department of Biological Sciences, Purdue University, West Lafayette, IN 47907-1392

Communicated by Michael G. Rossmann, Purdue University, West Lafayette, IN, August 14, 1995 (received for review June 28, 1995)

ABSTRACT **The structures of Sindbis virus and Ross River virus complexed with Fab fragments from monoclonal antibodies have been determined from cryoelectron micrographs. Both antibodies chosen for this study bind to regions of the virions that have been implicated in cell-receptor recognition and recognize epitopes on the E2 glycoprotein. The two structures show that the Fab fragments bind to the outermost tip of the trimeric envelope spike protein. Hence, the same region of both the Sindbis virus and Ross River virus envelope spike is composed of E2 and is involved in recognition of the cellular receptor.**

The alphaviruses are a group of 26 icosahedral, positive-sense RNA viruses (1) that are primarily transmitted by mosquitoes. These ≈700-Å-diameter viruses are some of the simplest of the membrane-enveloped viruses, and members of this group cause serious tropical diseases with characteristic symptoms such as myositis, fever, rash, encephalitis, and polyarthritis. We have studied two members of this group: Ross River virus (RR) and Sindbis virus (SIN). RR causes epidemic polyarthritis in humans and is endemic to Australia (2). SIN, first isolated in Sindbis, Egypt, causes an often lethal paralysis in neonatal mice. Laboratory SIN isolates are considered avirulent in humans, but natural variants from Northern Europe can cause polyarthritis (3).

The amino acid sequences of the RR and SIN virus structural and nonstructural proteins are 49% and 64% identical, respectively (4). The 3′ end of the genome codes for a subgenomic mRNA that is the template for a 138-kDa precursor polyprotein that is subsequently cleaved to form the four major structural proteins: the nucleocapsid protein (≈30 kDa) and the three envelope glycoproteins E1 (≈52 kDa), E2 (≈49 kDa), and E3 (≈10 kDa). The viral RNA genome and 240 copies of the capsid protein form the nucleocapsid core (5–10), and the E1 and E2 glycoproteins form heterodimers that associate as 80 trimeric spikes on the viral surface (8, 11–13). Native SIN and RR lack the E3 glycoprotein because it disassociates from the spike complex after its display on the plasma membrane surface (14, 15). E1 has a putative fusion domain that may facilitate host membrane penetration (16, 17). E2 contains most of the neutralizing epitopes and is also probably involved in host cell recognition (18–20). E1 and E2 both traverse the viral lipid bilayer, but only E2 has an extended cytoplasmic domain (31 and 33 residues in RR and SIN, respectively) that is thought to contact the nucleocapsid core (21, 22).

The atomic structure of an alphavirus has not yet been determined because the best crystals diffract x-rays to only ≈30-Å resolution (23). However, cryoelectron microscopy (cryo-EM) studies have helped define the basic architecture of Semliki Forest and SIN viruses (8, 12, 13). These techniques were recently used to produce an ≈25-Å resolution electron density map of RR that clearly showed the nucleocapsid and spike arrangement (Fig. 1) (10). The spike and capsid proteins are both arranged with T = 4 icosahedral symmetry. In the nucleocapsid, the core proteins form 12 pentamer and 30 hexamer capsomeres (Fig. 1*A*). The observable portion of the SIN core protein structure (6) nicely models this capsomeric density. Each trimeric spike has a clover-leaf shape with three bilobed (E1-E2) petals. Directly beneath each petal, density extends across the lipid bilayer and contacts a capsid protein monomer (Fig. 1*B*). At the icosahedral 3-fold axes, the three extensions from one spike contact three adjacent hexamers, whereas at the quasi 3-fold axes, the extensions contact one pentamer and two hexamers. Each spike has a hollow cavity in its center that is formed because the glycoproteins splay out from the base making a shell of density that covers most of the outer surface of the lipid bilayer. The hollow cores in the spikes might play a role in membrane fusion with the host (10). Subsequently, all of these structural details were also observed in the cryo-EM structure of Semliki Forest virus (24).

Here we describe the three-dimensional structures of RR and SIN, each complexed with Fab fragments that are believed to bind to the region of the spikes that are sites of cell-receptor attachment. Similar cryo-EM and image reconstruction studies on other virus/Fab and virus/antibody complexes have shown that these methods accurately reveal epitope–paratope interactions (25–30). The Fab fragments from SV209 (31) and T10C9 (32) (hybridoma cell line designations) bind in homologous positions on the tip of the trimeric spikes of SIN and RR, respectively. Thus, these two alphaviruses probably use similar regions of the spike envelope protein to recognize their respective host cell receptor. In addition, these results directly demonstrate that a portion of the E2 glycoprotein lies in the outermost region of the spike.

MATERIALS AND METHODS

Antibody Production and Fab Purification. Hybridoma cell lines that produce monoclonal antibodies to both RR (T10C9) (32) and SIN (SV209) (31) were grown in a Cellmax Quad 4 cell culture system (Cellco, Germantown, MD) using a hybridoma-MPS (moderate pore size) cartridge with a molecular mass cutoff of 30 kDa. Fluid from the chamber was collected, and the cellular debris was removed by centrifugation for 15 min at 10,000 × *g*. Antibodies were then precipitated from the supernatant with a 50% (final concentration) saturated ammonium sulfate solution. The precipitate was collected with a 15-min centrifugation at 10,000 × *g* and dialyzed against 0.1 M sodium phosphate buffer, pH 7.5. The antibodies were then purified with protein G affinity chromatography using 0.1 M sodium phosphate wash buffer, pH 7.5, and 50 mM sodium

The publication costs of this article were defrayed in part by page charge payment. This article must therefore be hereby marked "*advertisement*" in accordance with 18 U.S.C. §1734 solely to indicate this fact.

Abbreviations: RR, Ross River virus; SIN, Sindbis virus; cryoEM, cryoelectron microscopy.

*To whom reprint requests should be addressed.

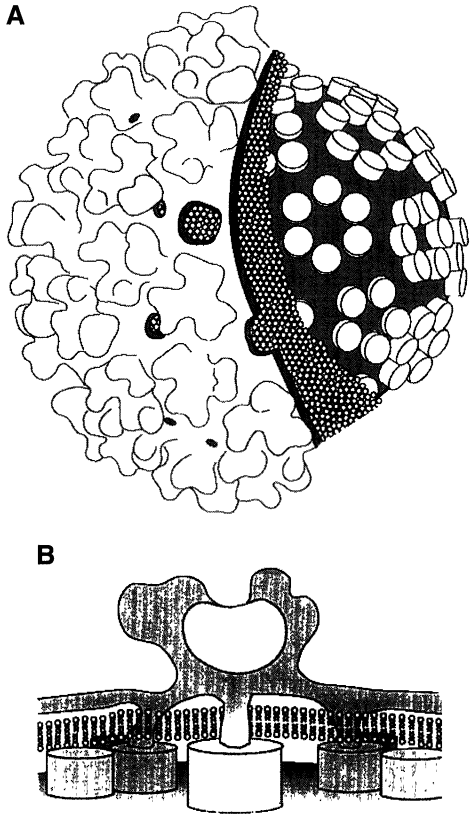

FIG. 1. Schematic diagram of the T = 4 RR structure (10). (*A*) Overall organization of RR. Shown on the left side is the outermost surface of RR composed of trimers of E1 and E2 envelope glycoproteins. The base of the trimeric spikes splay out to form a protein shell that covers the lipid bilayer (represented by small balls), except for small holes just outside the base of the spikes and on the icosahedral 5-fold axes and large holes at the icosahedral 2-fold axes. Beneath the shell lies the lipid bilayer that covers the T = 4 nucleocapsid core. The short barrels represent the ordered portion of the capsid protein, and these are arranged in hexamer and pentamer clusters. The shaded region represents a combination of the RNA and the "disordered" nucleocapsid protein in the reconstruction. (*B*) Schematic diagram of a trimeric spike and its interactions with the core protein below the bilayer membrane. A transmembrane domain extends from each of the three petals of the envelope spike and associates with core protein monomer.

acetate elution buffer, pH 2.0. SV209 was digested overnight with a 1:100 (wt/wt) ratio of papain/antibody, and T10C9 was digested for 4 hr with a 1:5000 (wt/wt) ratio of papain to antibody. Digestion was done at 37°C in the presence of 2-mercaptoethanol (25 mM for SV209 and 30 mM for T10C9) and then quenched with 75 mM iodoacetamide (final concentration). Digested antibody was then dialyzed against 20 mM Tris buffer, pH 7.5–7.8, and the Fab fragments were purified by using a Mono Q column attached to a fast protein liquid chromatography system. Under these conditions, only the Fab fragments eluted in the void volume.

Virus Production and Purification. The T48 strain of RR, rescued from the full-length cDNA clone pRR64, was used as the source of virus (33). Mosquito cell line C6/36 (*Aedes albopictus*) was used for propagation. Cells were grown at 30°C in roller bottles using Eagle minimal essential medium/10% fetal calf serum and were infected with virus at a multiplicity of one. After a 36-hr incubation, cell supernatants were harvested, and virus was concentrated by precipitation in 10% polyethylene glycol/0.5 M NaCl. The virus was resuspended and purified by sucrose density centrifugation.

The SB strain of SIN AR339 isolate (34) was propagated in monolayers of BHK cells at 37°C. The remaining protocol was the same as that used for RR, except a 20%/30% Na^+/K^+ tartrate step gradient was used instead of the sucrose gradient.

CryoEM and Image Reconstruction. Virus samples, at a final concentration of ≈1 mg/ml, were added to their cognate Fab fragments at a ratio of ≈960 Fab fragments/virion (approximately four Fab fragments per E1-E2 dimer) and incubated overnight at 4°C. Because of concerns about particle stability, excess Fabs were not removed by size-exclusion chromatography, as described in the Fab/HRV14 studies (26). Additional sodium chloride (≈100 mM final concentration) was added to inhibit aggregation because neither the Fabs nor the viruses were very soluble at concentrations necessary for microscopy.

Cryo-EM and image analysis procedures were essentially the same as those previously reported for a native RR sample (10). The sample was maintained at near liquid nitrogen temperature, and images were recorded under minimal dose conditions (≈10 $e^-/Å^2$), at 80 kV, at ≈ ×36,000 and with an objective lens underfocus between 1.0 and 1.4 μm. Particle images were first selected by visual inspection (35, 36) and then were further screened using a model-based approach that determined the relative orientations of the particles and provided quantitative criteria to select the best set of self-consistent image data (49). Data sets of 42 RR/Fab and 15 SIN/Fab particle images were used to compute the final three-dimensional reconstructions at resolutions of 25 and 32 Å, respectively, by use of the Fourier–Bessel method (24, 37). The absolute hand of each reconstruction was determined by comparison with the native RR structure (10).

RESULTS AND DISCUSSION

Properties of the Neutralizing Antibodies. The neutralizing antibodies chosen for these studies (SV209 and T10C9) are thought to bind to their respective viruses at or near the cell receptor recognition site on the E2 glycoproteins (31, 32). Antiidiotypic antibodies to SV209 compete with SIN for its cellular receptor and block viral attachment by ≈50% (19). These antiidiotypic antibodies to SV209 recognized 110-kDa and 74-kDa cellular proteins in N18 neuroblastoma cells,

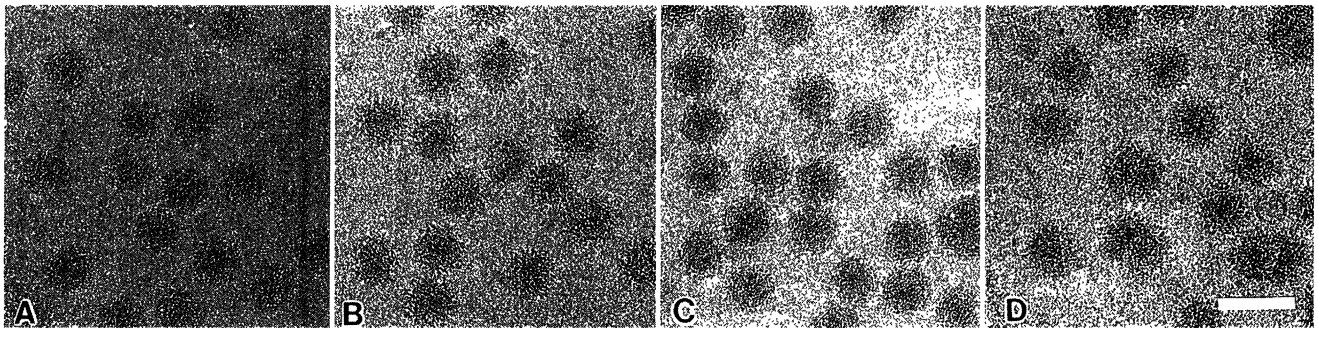

FIG. 2. Images of frozen-hydrated samples of native RR (*A*), Fab/RR (*B*), native SIN (*C*), and Fab/SIN (*D*). (Bar = 1000 Å.)

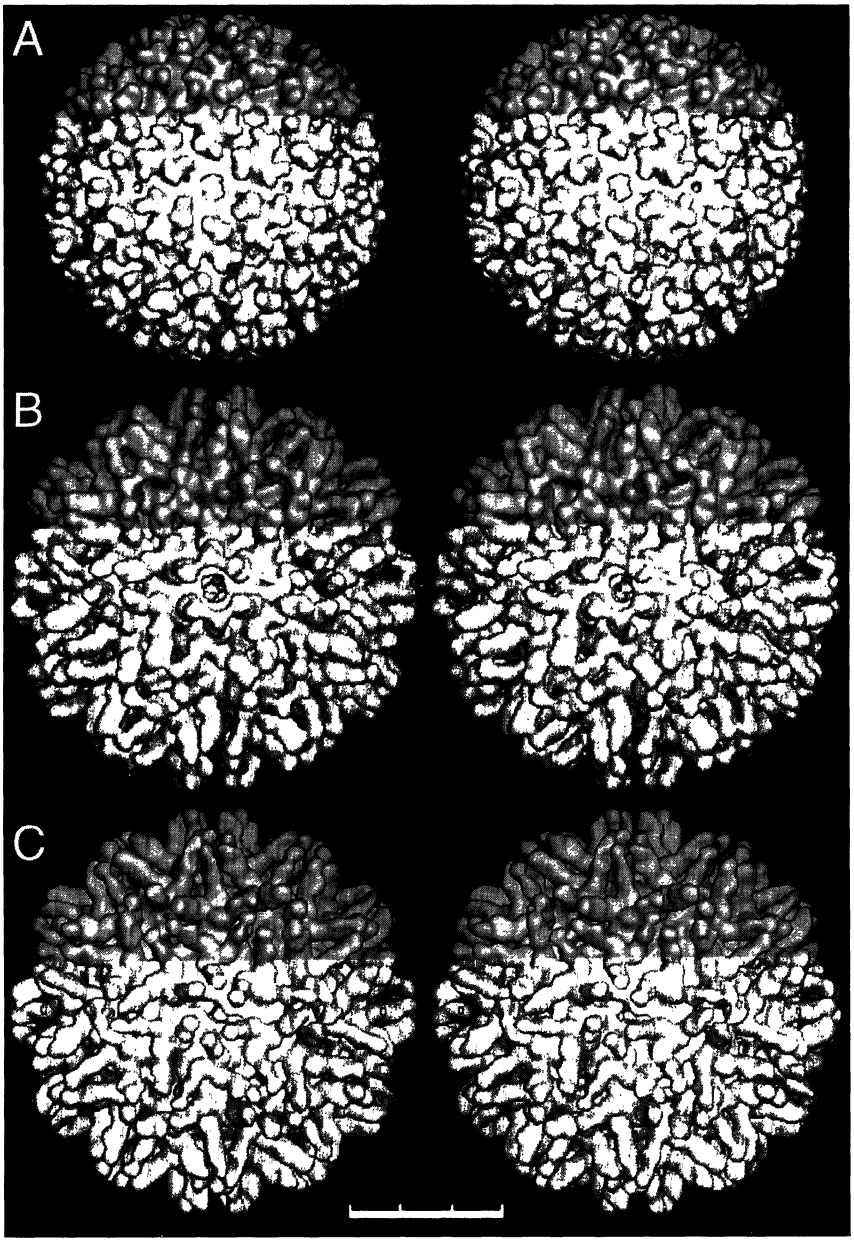

FIG. 3. Stereoviews of surface renderings of the cryo-EM image reconstructions of RR (*A*), RR/Fab (*B*), and SIN/Fab (*C*). The arrows in *B* show the view direction depicted in Fig. 4. (Bar = 300 Å.)

which presumably are receptors for SIN. Interestingly, the expression of the receptor proteins recognized by the antiidiotypic antibodies ceased in half of the brain cells in mice 4 days after birth, lending a possible explanation for the age-dependent nature of SIN neurovirulence (19). Although the identities of the 110-kDa and 74-kDa proteins are not known, another receptor for SIN on BHK cells has been identified as the high-affinity laminin receptor (38). This protein is highly conserved across species, suggesting that the wide host range of SIN may, in part, be due to its use of a ubiquitous protein on the surface of target cells. In addition, it appears that SIN uses multiple receptors to gain entry into cells, although the relationship between these proteins is not yet known.

The natural escape mutant to the T10C9 antibody maps to residue Thr-216 on the RR E2 glycoprotein (32). This residue is presumably near the cell receptor binding site because residue Asn-218 was found to vary as the virus adapted to growth in chicken cells (39). Site-specific amino acid substitutions at this residue affect the sensitivity of chicken cells to infection with RR (R. C. Weir, J. H. Strauss, and R.J.K., unpublished results). In addition, residue Thr-219 mutated to alanine during the course of an epidemic in humans (40). Because small mammals act as the viral reservoir in nature, this mutation may represent changes in E2 necessary to alter host specificity. Although mutations at these sites might induce conformational changes at distal sites, these results strongly support the notion that the region adjacent to this RR epitope (T216) is intimately involved in cell receptor recognition. Unlike SIN, no cellular receptors have yet been identified for RR.

Image Reconstructions of T10C9/RR and SV209/SIN Complexes. Images of the Fab/virus complexes clearly show the complexes to have a larger "halo" of density compared to native virus (Fig. 2). The virus and virus complex samples tended to aggregate (Fig. 2), and this problem greatly limited the number of particle images that could be included in the reconstructions. The RR/Fab structure was determined to 25-Å resolution from 42 images (Fig. 3*B*), and the structure of the SIN/Fab complex was determined to 32-Å resolution from 15 images (Fig. 3*C*). The native SIN particles (Fig. 2*C*) led to

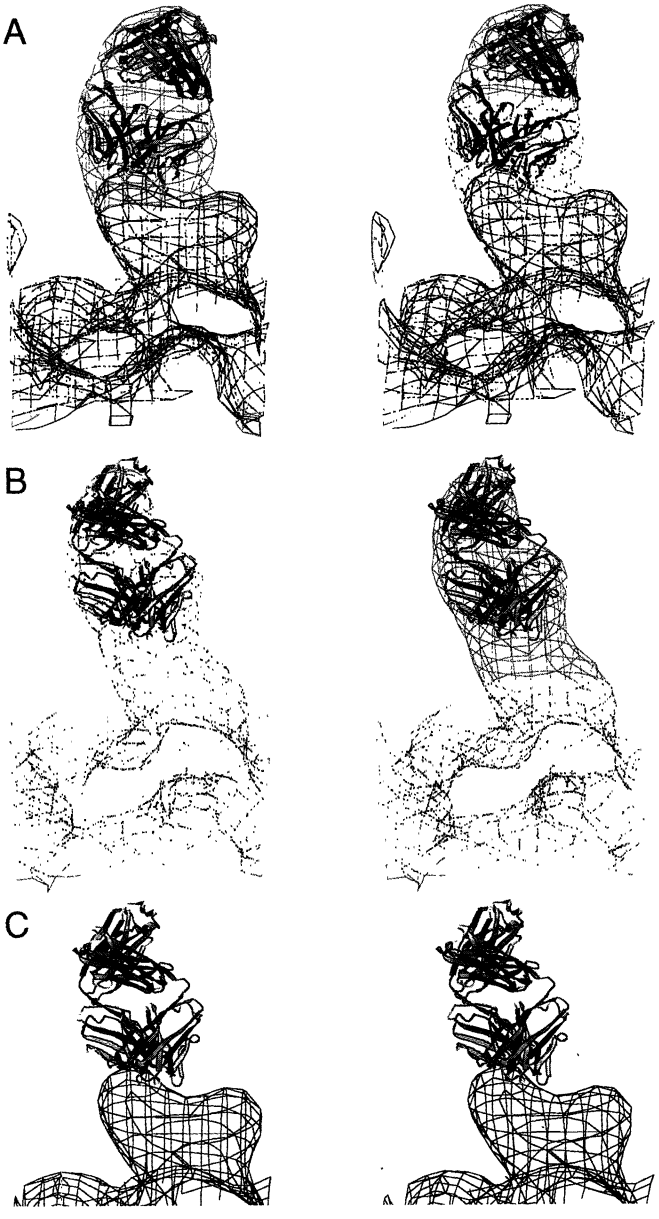

FIG. 4. Fit of the atomic structure of Fab17-IA into the corresponding Fab density in the RR/Fab (*A*) and SIN/Fab (*B*) reconstructions. The same view direction is used in *A–C* and is from a vantage point near the surface of the virion with the center of the virus toward the bottom of the diagram and looking face on toward one of the Fab molecules on the pseudo 3-fold spike (see arrows, Fig. 3*B*). The ribbon model of Fab17-IA has the light chain in blue and the heavy chain in red. The RR/Fab and SIN/Fab density is gray in *A* and *B*, respectively. To compare the Fab/virus contacts between the RR/Fab and SIN/Fab complexes, the electron density of the RR image reconstruction (green) is included in *A* and *C*.

a reconstruction of significantly lower quality than the native RR reconstruction (Figs. 2*A* and 3*A*). The SIN and SIN/Fab reconstructions were of lower quality than the respective RR reconstructions, and this is only partially attributable to the number of images used. SIN may be more unstable than RR as evident in lower icosahedral correlations measured by common lines and cross-common line phase residuals (37). Instability of SIN may reflect inherent differences between RR and SIN or might be caused by an unidentified destabilizing affect of the protocol used to purify SIN. The SIN/Fab reconstruction was superior to that of SIN alone. It is unclear why this was the case but may be due to some stabilization of the virions by the bound Fab fragments. Nonetheless, the basic structural features (spikes, membrane, nucleocapsid core) in the SIN and SIN/Fab reconstructions are directly comparable to the RR reconstructions.

In both virus/Fab reconstructions, the Fabs appear as bilobed structures that bind to the outermost tips of the trimeric spikes. The lobe in contact with the spike represents the Fab variable domain (V_H·V_L), and the distal lobe represents the Fab constant domain (C_{H1}·C_L). Both domains have approximately equal mass in the RR/Fab complex, but the constant domain has lower density than the variable domain in the SIN/Fab complex. The constant domains that are nearest to the pseudo-6-fold axes in the RR/Fab complex appear to merge with one another. Similar "contacts" occur in the SIN/Fab structure for the Fab constant domains that are nearest the 5-fold axes. This merging of the density is most likely a consequence of limited resolution in the EM data.

Modeling of an Fab Atomic Structure into the Image Reconstructions. The densities of the bound Fab fragments correlate well with the expected molecular envelope of a typical Fab structure. The atomic structures of several Fab fragments have been determined (for review, see ref. 41). Though the basic structures of the variable and constant domains of all Fab molecules are well conserved, the angle between these domains (the elbow angle) and the details of the paratopes greatly differ. At ≈25-Å resolution, it is possible to distinguish small differences in the elbow angle. The structure of Fab17-IA (from a neutralizing monoclonal antibody to human rhinovirus 14) (28), which has an elbow angle value commonly found in Fab structures (≈168°), was used to model the Fab density of both alphavirus/Fab complexes (Fig. 4). Fab17-IA was unambiguously placed in the RR/Fab map because the constant and variable domains and the angle between them are clearly represented in the reconstructed density. The weakness in the Fab constant domain in the SIN/Fab complex made it impossible to unambiguously assign an elbow angle, and therefore the orientation of the Fab as shown in Fig. 4*B* may actually be off by an ≈180° rotation about the long axis of the Fab. Comparison of the RR and RR/Fab electron densities revealed no significant differences, apart from the bound Fab (Fig. 4*A*). To highlight the similarities and differences in the binding of Fab fragments to RR and SIN, the fitted atomic models are shown along with a portion of the reconstructed RR spike density (Fig. 4 *A* and *C*). The RR rather than the SIN native spike density was used in Fig. 4*C* because the quality of the native RR reconstruction was significantly better than that of the native SIN reconstruction. The two Fabs clearly bind in different orientations, but they do so with nearly identical "footprints" (paratope–epitope interactions). In both Fab models, the three heavy-chain CDRs (complementarity-determining regions) and the CDR1 and CDR3 loops of the light chain contact the spike surface. The top portion of the rounded knob of the spike nicely fits into the cleft between the heavy and light chains. The heavy chain CDR3 loop in the SIN/Fab model protrudes slightly into the RR spike density. This overlap could reflect an error in placing the Fab into the SIN/Fab density, the Fab17-IA model may not accurately depict the SV209 antibody in this region, or the SIN spike morphology may differ from RR at this site.

Our results clearly demarcate key aspects of the spike topology. The outermost tip of the spike must be mostly composed of E2 because both SV209 and T10C9 recognize epitopes only on the E2 glycoprotein. This placement of E2 is consistent with previous reports that E1 forms the core of the trimeric spike and that E2 decorates the outer perimeter (42). However, the possibility that portions of E1 may also lie in this outermost lobe, as suggested by Vénien-Bryan and Fuller (43), is not excluded by these results. Because both antibodies are likely to bind at or near the cell receptor recognition region (19, 32, 40), it may be concluded that this outer lobe of the spike is involved in cellular recognition. The overlap between

the footprints of the T10C9 and SV209 antibodies also suggests that the portion of the spike used for host recognition is highly conserved among the two very different alphaviruses. However, it does not exclude the possibility of additional, nonoverlapping cell receptor recognition regions on either or both viruses. Finally, the Fab footprints directly map some of the key viral surfaces involved in attenuation, host recognition, and antibody neutralization.

The image reconstruction and atomic modeling provide a powerful hybrid approach to obtain pseudo-atomic details about large macromolecular complexes (25–30, 44–48), especially when crystals of such complexes are not available or do not diffract x-rays to high resolution. The structures of other Fab/alphavirus complexes will help map out further details of the spike topology. Once the atomic structures of the spike glycoproteins are determined, such information will be essential in assembling an accurate model for the intact virion.

We thank Diane Griffin for the generous gift of the SV209 antibody and Ron Weir and Lynn Dalgarno for the T10C9 antibody. This work was supported by National Institutes of Health (NIH) Grants AI33982 (R.J.K.) and GM33050 (T.S.B.) and National Science Foundation Grant MCB-9206305 (T.S.B.). T.J.S., R.J.K., and T.S.B. have also benefited from an NIH program project grant (AI35212) and from a Markey Grant for the development of structural studies at Purdue University.

1. Calisher, C. H., Karabatsos, N., Lazuick, J. S., Monath, T. & Wolff, K. L. (1988) *Am. J. Trop. Med. Hyg.* **38,** 447–452.
2. Kay, B. H. & Aaskov, J. G. (1989) in *The Arboviruses: Epidemiology and Ecology*, ed. Monath, T. T. (CRC, Boca Raton, FL), Vol. 4, pp. 93–112.
3. Niklasson, B., Aspmark, A., LeDuck, J. W., Gargan, T. P., Ennis, W. A., Tesh, R. B. & Main, A. J., Jr. (1984) *Am. J. Trop. Med. Hyg.* **33,** 1212–1217.
4. Strauss, J. H. & Strauss, E. G. (1994) *Microbiol. Rev.* **58,** 491–562.
5. Coombs, K. & Brown, D. T. (1987) *Virus Res.* **7,** 131–149.
6. Choi, H.-K., Tong, L., Minor, W., Dumas, P., Boege, U., Rossmann, M. G. & Wengler, G. (1991) *Nature (London)* **354,** 37–43.
7. Paredes, A. M., Simon, M. & Brown, D. T. (1993) *Virology* **187,** 324–332.
8. Paredes, A. M., Brown, D. T., Rothnagel, R., Chiu, W., Johnston, R. E. & Prasad, B. V. V. (1993) *Proc. Natl. Acad. Sci. USA* **90,** 9095–9099.
9. Tong, L., Wengler, G. & Rossmann, M. G. (1993) *J. Mol. Biol.* **230,** 228–247.
10. Cheng, R. H., Kuhn, R. J., Olson, N. H., Rossmann, M. G., Choi, H., Smith, T. J. & Baker, T. S. (1995) *Cell* **80,** 621–630.
11. von Bonsdorff, C.-H. & Harrison, S. C. (1975) *J. Virol.* **16,** 141–145.
12. Vogel, R. H., Provencher, S. W., von Bonsdorff, C. H., Adrian, M. & Dubochet, J. (1986) *Nature (London)* **320,** 533–535.
13. Fuller, S. D. (1987) *Cell* **48,** 923–934.
14. Mayne, J. T., Rice, C. R., Strauss, E. G., Hunkapiller, M. W. & Strauss, J. H. (1984) *Virology* **134,** 338–357.
15. Vrati, S., Faragher, S. G., Weir, R. C. & Dalgarno, L. (1986) *Virology* **151,** 222–232.
16. Garoff, H., Frischauf, A. M., Simons, K., Lehrach, H. & Delius, H. (1980) *Proc. Natl. Acad. Sci. USA* **77,** 6376–6380.
17. Rice, C. M. & Strauss, J. H. (1981) *Proc. Natl. Acad. Sci. USA* **78,** 2062–2066.
18. Strauss, E. G., Stec, D. S., Schmaljohn, A. L. & Strauss, J. H. (1991) *J. Virol.* **65,** 4654–4664.
19. Ubol, S. & Griffin, D. E. (1991) *J. Virol.* **65,** 6913–6921.
20. Wang, K.-S., Schmaljohn, A. L., Kuhn, R. J. & Strauss, J. H. (1991) *Virology* **181,** 694–702.
21. Garoff, H. & Simons, K. (1974) *Proc. Natl. Acad. Sci. USA* **71,** 3988–3992.
22. Lopez, S., Yao, J.-S., Kuhn, R. J., Strauss, E. G. & Strauss, J. H. (1994) *J. Virol.* **68,** 1316–1323.
23. Harrison, S. C., Strong, R. K., Schlesinger, S. & Schlesinger, M. J. (1992) *J. Mol. Biol.* **226,** 277–280.
24. Fuller, S. D., Berriman, J. A., Butcher, S. J. & Gowen, B. E. (1995) *Cell* **81,** 715–725.
25. Wang, P., Porta, C., Chen, Z., Baker, T. S. & Johnson, J. E. (1992) *Nature (London)* **355,** 275–278.
26. Smith, T. J., Olson, N. H., Cheng, R. H., Liu, H., Chase, E., Lee, W. M., Leippe, D. M., Mosser, A. G., Ruekert, R. R. & Baker, T. S. (1993) *J. Virol.* **67,** 1148–1158.
27. Smith, T. J., Olson, N. H., Cheng, R. H., Chase, E. S. & Baker, T. S. (1993) *Proc. Natl. Acad. Sci. USA* **90,** 7015–7018.
28. Liu, H., Smith, T. J., Lee, W. M., Leippe, D., Mosser, A. & Rueckert, R. R. (1994) *J. Mol. Biol.* **240,** 127–137.
29. Wikoff, W. R., Wang, G., Parrish, C. R., Cheng, R. H., Strassheim, M. L., Baker, T. S. & Rossmann, M. G. (1994) *Structure* **2,** 595–607.
30. Porta, C., Cheng, R. H., Chen, Z., Baker, T. S. & Johnson, J. E. (1994) *Virology* **204,** 777–788.
31. Mendoza, Q. P., Stanley, J. & Griffin, D. E. (1988) *J. Gen. Virol.* **70,** 3015–3022.
32. Vrati, S., Fernon, C. A., Dalgarno, L. & Weir, R. C. (1988) *Virology* **162,** 346–353.
33. Kuhn, R. J., Niesters, H. G. M., Hong, Z. & Strauss, J. H. (1991) *Virology* **182,** 430–441.
34. Davis, N. L., Pence, D. F., Meyer, W. J., Schmaljohn, A. L. & Johnson, R. E. (1987) *Virology* **161,** 101–108.
35. Baker, T. S., Newcomb, W. W., Olson, N. H., Cowsert, L. M., Olson, C. & Brown, J. C. (1991) *Cell* **60,** 1007–1015.
36. Cheng, R. H., Olson, N. H. & Baker, T. S. (1992) *Virology* **186,** 655–668.
37. Crowther, R. A. (1971) *Philos. Trans. R. Soc. London B* **261,** 221–230.
38. Wang, K.-S., Kuhn, R. J., Strauss, E. G., Ou, S. & Strauss, J. H. (1992) *J. Virol.* **66,** 4992–5001.
39. Kerr, P. J., Weir, R. C. & Dalgarno, L. (1993) *Virology* **193,** 446–449.
40. Burness, A. T., Pardoe, I., Faragher, S. G., Vrati, S. & Dalgarno, L. (1988) *Virology* **167,** 639–643.
41. Kabat, E. A., Wu, T. T., Reid-Miller, M., Perry, H. M. & Gottesman, K. S. (1987) in *Sequences of Proteins of Immunological Interests* (Natl. Inst. Health, Bethesda).
42. Anthony, R. P. & Brown, D. T. (1991) *J. Virol.* **65,** 1187–1194.
43. Vénien-Bryan, C. & Fuller, S. D. (1994) *J. Mol. Biol.* **236,** 572–583.
44. McKenna, R., Xia, D., Willingman, P., Ilag, L. L., Krishaswamy, S., Rossmann, M. G., Olson, N. H., Baker, T. S. & Incardona, N. L. (1992) *Nature (London)* **355,** 137–143.
45. Stewart, P. L., Fuller, S. D. & Burnett, R. M. (1993) *EMBO J.* **12,** 2589–2599.
46. Cheng, R. H., Reddy, V., Olson, N. H., Fisher, A., Baker, T. S. & Johnson, J. E. (1994) *Structure* **2,** 271–282.
47. Ilag, L. L., Olson, N. H., Dokland, T., Music, C. L., Cheng, R. H., Bowen, Z., McKenna, R., Rossmann, M. G., Baker, T. S. & Incardona, N. L. (1995) *Structure* **3,** 353–363.
48. Speir, J. A., Munshi, S., Wang, G., Baker, T. S. & Johnson, J. E. (1995) *Structure* **3,** 63–78.
49. Baker, T. S. & Cheng, R. H. (1995) *J. Struct. Biol.*, in press.